Mon. Not. R. Astron. Soc. **000**, 000–000 (0000) Printed 23 August 2002 (MN LaTeX style file v2.2)

Spectropolarimetry of O supergiants

Tim J. Harries[1], Ian D. Howarth[2], and Christopher J. Evans[2]
[1]*School of Physics, University of Exeter, Stocker Road, Exeter EX4 4QL.*
[2]*Department of Physics and Astronomy, University College London, Gower Street, London WC1E 6BT, England.*

Dates to be inserted

ABSTRACT

We present medium-resolution spectropolarimetry at high signal to noise of the Hα emission line of 20 O-type supergiants. Five stars (25%) of the sample show a statistically significant change in polarization through the line.

We combine our Hα data with new K-band spectropolarimetry and archival low-resolution optical spectropolarimetry to determine the polarigenic mechanism in the stars that show a line effect. We show that the line polarization change in the binary systems is due to the classical 'dilution' mechanism, in which the Hα emission is essentially unpolarized and the continuum polarization is due to intra-binary scattering. We find that the line effect in HD 108 is also well modelled by pure dilution, but suggest the continuum polarization is the result of stochastic wind clumping. A similar description applies to the continuuum polarization of HD 188001, although the line effect cannot be reproduced by pure dilution. We use low-resolution spectropolarimetry to determine the interstellar polarization vector to λ Cephei, and confirm that the intrinsic polarization of the object is very low (< 0.1%, corresponding to an equator:pole density ratio of < 1.25). The line polarization of this star is modelled by using the TORUS three-dimensional radiative-transfer code (Harries 2000). We show that the line effect is a consequence of symmetry breaking due to the system's rapid ($> 200\,\mathrm{km\,s^{-1}}$) rotation, and that the system is polarimetrically similar to the O4 supergiant ζ Puppis.

Finally, we note that the precision of current photo- and spectro-polarimetric observations is insufficient to test structured wind models, which predict a continuum polarization of ~ 0.1 per cent.

Key words: Stars – Stars: mass-loss – Polarization

1 INTRODUCTION

At critical periods in their evolution, the most massive stars exhibit prodigious stellar winds, driven by the pressure of the intense radiation field mediated by resonant scattering. Hydrodynamical models of radiation-driven winds (e.g., Castor, Abbott & Klein 1975; Pauldrach, Puls & Kudritzki 1986) have been remarkably successful in predicting many of the observable quantities of the stellar winds such as the mass-loss rates and terminal velocities (e.g., Howarth & Prinja 1989, Pauldrach et al. 1994; Puls et al. 1996).

Standard diagnostics of mass loss assume steady-state, spherically symmetric outflows. However, O stars as a class are rapid rotators (Conti & Ebbetts 1977; Howarth et al. 1997), and there are both observational and theoretical grounds for expecting rotation to modify wind structure. Models of rotating, cylindrically symmetric, radiation-driven winds suggest that, compared to polar outflows, rotating stars eject more mass at slower speeds at their equators, due to the lower surface gravity there (e.g. Friend & Abbott 1986; Pauldrach, Puls & Kudritzki 1986), while at the extreme end of the rotation distribution it is possible that wind compression may play a rôle, with streamlines from the 'upper' and 'lower' hemispheres converging at the equator and producing a disk (Bjorkman & Cassinelli 1994; but see also Owocki, Cranmer & Gayley 1996).

Observational diagnostics for departures from wind sphericity are often quite subtle. Variability in UV resonance lines has been observed to occur on timescales indistinguishable from the rotation period in some systems (e.g., Howarth, Prinja & Massa 1995), suggesting large-scale *azimuthal* asymmetries, and among the most rapid rotators are stars showing profile morphology that can be interpreted as the result of a latitudinal density- and velocity-law dependence (Howarth & Reid 1993, Howarth et al. 1997). However, the most compelling evidence for large-scale departures from spherical symmetry comes from polarization measurements, which provide a direct (if not unique) probe of the electron distribution about the star.

The earliest indications of asymmetries in the distribution of electron-scattered photons came from photometric observations of variable polarization in early-type stars (e.g., Serkowski 1968; Hayes 1975). However, such observations can only probe the time-dependent element of any intrinsic polarization. For steady-state structure, spectropolarimetry of emission lines affords a particularly powerful diagnostic tool: the continuum is polarized by photospheric photons Thomson-scattering off electrons in the stellar wind. The emission-line flux, produced in the outflow, 'sees' a smaller electron-scattering optical depth and is therefore less polarized, leading to a reduction in polarization magnitude at the emission-line wavelength. This so-called 'line effect' has been observed in Wolf-Rayet stars (e.g. McLean 1980; Schulte-Ladbeck et al. 1992), Be stars (e.g. McLean et al. 1979), B[e] systems (e.g. Oudmaijer & Drew 1999), and Luminous Blue Variables (e.g. Schulte-Ladbeck et al. 1994).

A line effect was first reported in an O star by Harries & Howarth (1996b, hereinafter Paper I), who conducted a case study of Hα emission in the archetypal early-O supergiant ζ Puppis (O4 I(n)f; Walborn 1972). The results were interpreted in the context of a global wind asymmetry, with the equatorial outflow 2–3 times as dense as the polar outflow at a given height above the photosphere – a greater density contrast than predicted from simple '1-D' canonical radiation-driven wind theory.

Harries, Hillier & Howarth (1998) subsequently investigated the polarization characteristics of a sample of Wolf-Rayet (WR) stars. It was shown that about 15–20% of these stars have intrinsic polarizations greater than ~ 0.3 per cent, which corresponds to an equator:pole density ratio of 2–3 (similar to that of ζ Puppis) for an assumed, but plausible, parameterization of the wind geometry. It was postulated that those stars showing a detectable intrinsic polarization may represent the most rapidly rotating WR stars.

Recently Harries (2000) presented synthetic polarized line profiles of O stars computed using a new 3-dimensional radiative transfer code, TORUS. It was shown that although depolarization due to asymmetries was the dominant mechanism associated with the line-profile morphology, rotational velocity fields could also result in a change in polarization through Hα due to a breaking of the scattering symmetry in velocity space. It was found that for ζ Puppis the observed polarization signature was better matched by the new rotational effect than by traditional line depolarization.

In order to evaluate the frequency of observable line effects in O supergiants, and to investigate their implications and diagnostic potential, we have conducted spectropolarimetry of a small sample of bright O-supergiant stars. In the following section we describe these observations, and we then present our analysis and discuss our findings.

2 OBSERVATIONS AND DATA REDUCTION

2.1 Optical observations

The targets were selected on the basis of brightness, observability (i.e., celestial co-ordinates), and Hα line strength. The first set of observations was obtained on 1997 June 5 using the 3.9-m Anglo-Australian Telescope equipped with the RGO cassegrain spectrograph, 25-cm camera, 1200R grating, and a TEK CCD detector. This configuration provided a mean reciprocal dispersion of 0.9Å px^{-1} and a measured resolution of 1.3Å (which fully resolves the Hα emission-line profiles). The second set of observations was made during 1998 August 7–10 with the 4.2-m William Herschel Telescope used in conjunction with the ISIS dual-beam cassegrain spectrograph, 1200R grating, and a TEK CCD. (Only the red arm was used for the polarization observations.) The mean reciprocal dispersion of the WHT setup was 0.4Å px^{-1}, at a measured resolution of 0.9Å. In each spectrograph the polarimetry module is of similar construction, consisting of a rotating superachromatic half-wave retarder plate and a calcite analyzer.

Similar observing procedures were adopted at both sites. The dekker used on the RGO spectrograph has a pair of apertures, 'A' and 'B', for the sky and target, while the dekker used on ISIS has a 'comb', of which two apertures were designated 'A' and 'B'. Each polarization measurement consisted of a set of four exposures (corresponding to the 0°, 45°, 22.5° and 67.5° positions of the half-wave plate). A typical observation consisted of four sets of four exposures in an A-B-B-A aperture sequence. Observations of zero-polarization standards were obtained in the course of each run in order to calibrate the instrumental polarization, and of polarized standards to calibrate the position-angle (PA) offset of the instrument. Additional observations of zero-polarized standards were made through a polaroid filter to check the polarization efficiency. For the altazimuth-mounted WHT we set the position angle of the slit to the parallactic angle at the start of the (short) exposure in order to minimize the effects of atmospheric dispersion; the instrument was then rotated to maintain constant slit PA during the exposure, with the offset of the instrumental reference frame with respect to the celestial frame noted for each observation.

Preliminary data reduction (debiasing, flatfielding, cosmic-ray removal) was performed by using the FIGARO package (Shortridge et al. 1998). The polarization spectra were extracted using the software described by Harries & Howarth (1996a). The polarization calibration of the spectra was performed using the POLMAP package (Harries 1996). This involved removing the slight low-frequency wavelength-dependent position-angle error by a low-order polynomial fit to the PA of the polaroid-filter spectrum; rotating from the instrumental to celestial reference frame (WHT only); and rotating by an instrumental PA offset derived from observations of polarized standards. The magnitude of instrumental polarization, obtained from the zero-polarization standards, was found to be less than 0.1% for both instruments and was not corrected for, as flexure and other effects can introduce short-timescale zero-point drifts at this level of precision. The final spectra typically have 10^6–10^7 detected photons per pixel in the continuum, and are plotted in Fig. 3.

2.2 The spectropolarimetric ripple

Spectropolarimetry obtained with sufficiently high resolution and signal-to-noise has been demonstrated to show a $\sim$periodic instrumental signal, or 'ripple', in the Q and U

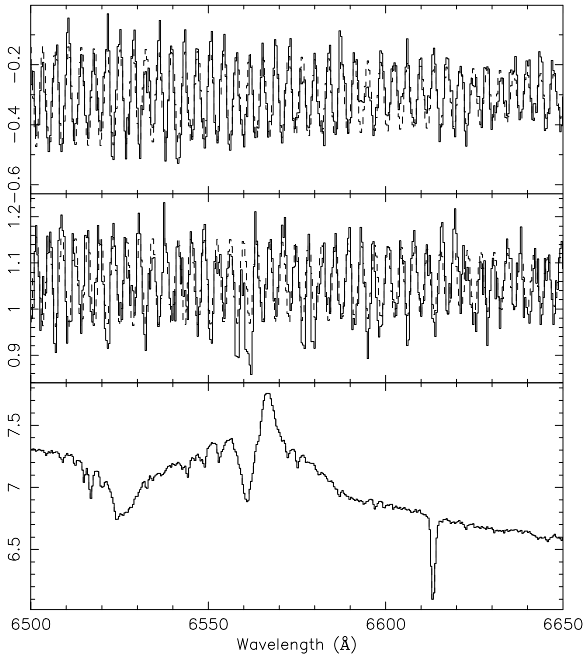

Figure 1. Raw spectropolarimetry of HD 210839 (λ Cep). The upper panels show the observed normalized Stokes parameters (solid lines), together with the model fit to the 'ripple' (dashed lines; cf. eqtn. 1 and Table 1).

Table 1. The results of the fit of eqtn. 1 to the WHT polarization spectra of HD 210839 (λ Cep) compared with the results of a similar fit to an AAT spectrum of HD 66811 (ζ Puppis; Paper I).

Parameter		WHT (HD 210839)			AAT (HD 66811)		
k	$\overline{q}$	0.174	$\pm$	0.004	0.073	$\pm$	0.01
	$\overline{u}$	0.097	$\pm$	0.003	0.082	$\pm$	0.01
p_1	$\overline{q}$	1056	$\pm$	80	1124	$\pm$	15
	$\overline{u}$	928	$\pm$	76	1141	$\pm$	14
p_2	$\overline{q}$	3.495	$\pm$	0.002	3.5563	$\pm$	0.0003
	$\overline{u}$	3.500	$\pm$	0.003	3.5593	$\pm$	0.0002
x_1	$\overline{q}$	6457	$\pm$	14	6455	$\pm$	3
	$\overline{u}$	6505	$\pm$	09	6447	$\pm$	3
x_2	$\overline{q}$	6400.37	$\pm$	0.03	6449.10	$\pm$	0.01
	$\overline{u}$	6402.00	$\pm$	0.05	6448.60	$\pm$	0.01
α	$\overline{q}$	1.592	$\pm$	0.002	1.596	$\pm$	0.002
(10^{-4})	$\overline{u}$	1.600	$\pm$	0.003	1.581	$\pm$	0.002

Stokes parameters, in both WHT and AAT data (Tinbergen 1994; Paper I). We find the peak-to-peak amplitude of the ripple is to be 0.1–0.2% for our AAT data, and 0.2–0.3% for the WHT, with the amplitude a function of wavelength. In both datasets the period of the ripple is about 3.5Å, with the ripple period increasing with wavelength. Investigation of this effect suggests that the likely cause is interference in the half-wave plate, which has a layered construction to achieve achromacity (Paper I).

For the data analyzed in Paper I, a satisfactory analytical representation of the ripple was found to be given by a 'chirp' function,

$$\overline{s}(\lambda) = k\cos\left(2\pi\frac{\lambda - x_1}{p_1}\right)\cos\left(2\pi\frac{\lambda - x_2}{p_2(1+\alpha(\lambda - x_2))}\right) + c_{\rm i}, \quad (1)$$

where $\overline{s}(\lambda)$ is the normalized Stokes parameter ($\overline{q} = Q/I$ or $\overline{u} = U/I$), k is the ripple semi-amplitude, x_1 and p_1 are the wavelength of the maximum amplitude and the period of the lower-frequency modulation, x_2 and p_2 are the wavelength of a maximum and the period of the high-frequency ripple, α is a slope parameter for the chirp, and $c_{\rm i}$ is the mean polarization. (The implicit assumption of constant continuum polarization over the spectral region under analysis is entirely satisfactory considering the narrow wavelength span of our data.)

We were able to correct our new spectropolarimetry adequately for the ripple by fitting eqtn. 1 to the spectra (excluding the region in the immediate vicinity of the Hα line) by using non-linear least-squares (Marquardt minimization). This functional form generally gives a good fit to the data, as illustrated in Fig. 1 for the WHT observations of HD 210839 (λ Cep). Comparing the results of this fit with that obtained for the AAT spectropolarimetry of ζ Puppis presented in Paper I, we find good agreement between the p_1, p_2, x_1, and α parameters (Table 1); this supports our original interpretation that it is the half-wave plate (which has the same construction and manufacturer at both the AAT and WHT) that is responsible for the instrumental ripple.

Donati et al. (1999) report similar ripple effects in a third half-wave plate built to the same specifications, but the ripple appears more complex and multi-periodic at the echelle spectral resolution of 35 000 they used.

2.3 Infrared measurements

Additional spectropolarimetric measurements were obtained on 1999 September 12/13, and 1999 October 10 by using the 3.8-m United Kingdom Infrared Telescope. The CGS4 spectrograph was used with the 150 l mm^{-1} grating and the 300mm camera, and a FPA46 array was employed as the detector. The polarization optics comprised a superachromatic (JHK) half-wave plate modulator and a MgF_2 Wollaston prism analyser. The central wavelength choosen was that of Brγ (2.165μm), and the setup provided spectral coverage from 2.1280 to 2.2090μm at a resolution of $5\times10^{-4}\mu$m. A 3×2 sampling scheme was used in order to Nyquist sample the spectrum and eliminate bad pixels, and a single polarimetric observation consisted of source and offset exposures at each of the four (0, 45, 22.5, 67.5 degree) half-wave plate orientations.

Preliminary data reduction was performed by using CGS4DR, which interlaced the subsampled images and removed bad pixels. The images were then resampled in order to remove the cross-dispersion tilt, which occurs because the slit is not perpendicular to the disperion direction. The ordinary and extraordinary intensity spectra were extracted by using software developed by us and based on the optimal extraction algorithm (Horne 1986), and the polarization vectors were computed using the ratio method (Tinbergen & Rutten 1992).

Unfortunately the extracted polarimetry was severely contaminated by polarimetric ripple, which originates from the half-wave plate as in the optical (see Section 2.2). Fourier analysis of the ripple demonstrated that it was dominated by two frequencies, and hence the fitting function used to correct the optical data was not applicable to our K-band observations. We therefore used Fourier filtering to reduce the level of the ripple, which necessarily compromised the spectropolarimetric information.

The final calibration of the data involved correction for the instrumental polarization and PA offset. We made a total of 7 observations of 5 different zero-polarization standard stars, which yielded a mean instrumental polarization of 0.1% at a PA of 115°. After subtracting this vector from all our observations, we found the mean instrumental PA offset (determined from observations of 4 polarized standard stars) to be 7°. We note that our observation of the polarized standard Taurus Elias 1 gave a PA offset that was significantly different to the other polarized standards, possibly indicating that this standard is variable.

A total of 5 of the O stars observed in the optical were observed during the UKIRT run, and the integrated continuum polarizations (approximately K-band photopolarimetry) of these are listed in Table 3.

3 OBSERVED POLARIZATION

3.1 Continuum polarization

We measured the observed continuum polarizations for the targets by summing the Stokes intensities over predefined wavelength bins (6200Å–6400Å & 6700Å–6900Å for the AAT data, and 6400Å–6500Å & 6600Å–6750Å for the WHT targets). These wavelengths correspond approximately to Johnson R, and the observed values, P_R, θ_R, are listed in Table 2. Although photon statistics alone suggest very small errors on these measurements (on the order of 0.001%), *absolute* measurements are only accurate to ±0.1% due to systematic effects, such as variations in instrumental polarization on short time-scales.

Previous photopolarimetric observations of our targets are included in Table 2 ($P_{\rm p}, \theta_{\rm p}$). Although photopolarimetry is not always available in our wavelength region any intrinsic (electron-scattering) polarization is grey across the optical region, while eqtn. 2, discussed in section 3.2, indicates that the ratio of interstellar polarizations at R and V differs from unity by less than 10% for $\lambda_{\rm max}$ in the range 0.4–0.75μm (3% for the 'standard' $\lambda_{\rm max} \simeq 0.55\mu$m), implying that comparisons with published V-band photopolarimetry can provide a useful guide to possible polarization variables.

The data in Table 2 show that there is generally excellent agreement between our observations and published photopolarimetry. Excluding the three BD-catalogue stars, which may show substantial polarimetric variability (see section 3.3), the mean differences $P_{\rm p} - P_{\rm o}$ are $+0.21 \pm 0.38$% for photopolarimetry from Hiltner (1956; $+0.12 \pm 0.29$% if HD 15570 is excluded), and $+0.05 \pm 0.08$% for all other sources. These statistics indicate that intrinsic variability in polarization magnitude must typically be less than ∼0.1% in normal O-type stars, confirming that any variability in the intrinsic polarization of O-type stars must normally be small (cf. Hayes 1978, 1984; Lupie & Nordsieck 1987; McDavid 2000; Clarke et al. 2002).

Table 3. K-band polarization measurements of O-supergiant stars obtained using UKIRT. The measurements are an intensity weighted mean polarization over the entire wavelength range (2.1280 to 2.2090μm). The errors given are formal errors according to photon statistics, and the true errors in $\overline{q}$ and $\overline{u}$ are approximately 0.1%. Also listed are the corresonding optical spectropolarimetric measurements.

Object	P (%)	θ (°)	P_R (%)	θ_R (°)
HD 14947	0.944 ± 0.015	129.2 ± 0.4	4.1	123
HD 188001	0.463 ± 0.013	28.4 ± 0.8	1.1	24
HD 190429A	0.261 ± 0.013	120.2 ± 1.4	0.6	108
HD 195592	0.264 ± 0.013	113.3 ± 1.4	1.1	118
HD 210839	0.204 ± 0.012	59.3 ± 1.7	1.1	55

3.2 Interstellar polarization

Appreciably reddened objects show linear polarization resulting from dichroic absorption by dust grains aligned in the Galactic magnetic field. The magnitude of this foreground interstellar polarization (ISP) scales approximately with A_V, and has a wavelength dependence which is well modelled by the empirical modified Serkowski's law,

$$p(\lambda)/p(\lambda_{\rm max}) = \exp\left[-K \ln^2\left(\lambda_{\rm max}/\lambda\right)\right], \qquad (2)$$

where $\lambda_{\rm max}$ is the wavelength of maximum polarization (in μm) and $K \simeq 1.7\lambda_{\rm max}$ (Serkowski, Mathewson & Ford 1975; Whittet et al. 1992); typically $\lambda_{\rm max} \sim 0.5$–$0.6\mu$m.

In order to examine the intrinsic polarization of the targets, it is first necessary to estimate the ISP vector. The most generally applicable method is to examine the polarization distribution of field stars, assuming that those field stars are themselves unpolarized, and that the ISP pattern does not vary over small spatial scales.

We searched the catalogue of Mathewson et al. (1978) for stars lying within 5° of each target on the plane of the sky. The distances to these stars were then estimated using a variety of photometric calibrations (see Harries & Howarth 1996a for details), while the distances to the targets were taken from Garmany's unpublished O-star catalogue (cf. Garmany, Conti & Chiosi 1982). We then selected field stars within ±2 magnitudes of the distance modulus of the target (more in some cases) to map out the ISP in each sightline. The ISP maps around the targets are illustrated in Fig. 4, along with the targets' observed continuum polarizations. (Although Mathewson et al. usually catalogue B-band photopolarimetric results, as noted previously $p(B)$ is expected to be within 10% of $p(R)$ for a Serkowski law with $\lambda_{\rm max}$ in the range 0.5–0.6μm, and differences in PA are expected to be negligible in most cases.)

The pattern of the ISP appears to be well-ordered along some sightlines (see, for example, Figs 4*e*, *f*, and *q*) but disordered along others (Figs 4*a*, *m*, and *p*). Unfortunately, most of the field stars that are co-spatial with the targets are themselves OB giants or supergiants which may show intrinsic polarization. We can, however, reasonably suppose that for those systems where the match is good the continuum polarization is dominated by the interstellar component, and that any intrinsic polarization is relatively small.

Table 2. Continuum polarization measurements of the sample. The third column indicates whether the target is a known binary ('B') or not ('S'), primarily based on the compilation by Mason et al. (1998). $P_{\rm R}$ [θ_R], $P_{\rm p}$ [$\theta_{\rm p}$], and $P_{\rm i}$ [$\theta_{\rm i}$] are our spectropolarimetric, published photopolarimetric, and adopted interstellar percentage polarizations [position angles, measured in degrees in the equatorial system], respectively; R- or V-band photopolarimetry is listed in preference to measurements in other regions. Observations on JD ...50605 were obtained at the AAT, and the remainder at the WHT.

Object	Spectral type	S/B	JD (−2400000)	$P_{\rm o}$ (Specpol.)	$\theta_{\rm o}$	$P_{\rm p}$ (Photopol.)	$\theta_{\rm p}$	λ	$P_{\rm i}$	$\theta_{\rm i}$	Sources
HD 108	O6: f?pe	S	51033	1.8	80						C
			51034	1.8	80						
			total	1.8	80	1.6	81	V	2.5	102	2
HD 14947	O5 I f+	S	51033	4.2	121						D
			51035	4.1	123						
			total	4.1	123	4.8	122	V	3.6	113	2
HD 15570	O4 I f+	S	51033	5.6	116						C
			51035	5.6	121	5.4	118	R			1
			total	5.5	120	6.4	117	V	3.7	114	2
HD 30614	O9.5 Ia	S	51033	1.4	137						F
(α Cam)			51034	1.4	137						
			total	1.4	137	1.5	135	R			5
HD 149404	O9 Ia	B	50605	3.1	3	3.2	3	V	0.7	32	F, 9
(V918 Sco)											
HD 151804	O8 Iaf	S	50605	1.2	47	1.2	46	V	0.9	37	C, 11
HD 152408	O8: Ia fpe	S	50605	0.7	40	0.7	39	···	0.9	37	C, 12
HD 153919	O6.5 Ia f+	B	50605	2.5	13	2.5	11	V	0.4	24	D, 7
(V884 Sco)											
HD 163758	O6.5 Ia f	S	50605	1.3	180	1.5	3	B	0.6	3	D, 3
HD 167971	O8 Ib (f)p	B	50605	1.0	147	1.3	150	V	1.0	46	C, 2
(MY Ser)											
HD 188001	O7.5 Ia f	S	51034	1.1	24	1.2	27	V	0.2	23	C, 10
(9 Sge)						1.1	29	R			5
HD 190429A	O4 I f+	S	51034	0.6	108				0.4	176	D
HD 192639	O7 Ib (f)	S	51035	0.4	9	0.2	···	V	0.2	160	C, 2
HD 195592	O9.7 Ia	S	51034	1.1	117						C
			51035	1.1	118						
			total	1.1	118	1.3	117	V	0.5	19	2
HD 202124	O9.5 Iab	S	51033	0.5	81				0.2	29	F
			51036	0.5	81						
			total	0.5	81	0.5	90	V			2
HD 210809	O9 Iab	S	51036	1.4	53	1.5	49	V	0.6	41	F, 2
HD 210839	O6 I (n)fp	S	51033	1.1	56				1.4	57	D
(λ Cep)			51035	1.1	53						
			51036	1.2	55	1.2	58	R			5
			total	1.1	55	1.2	59	V			2
BD+36 4063	O9.5Ib	B	51033	4.4	48	4.8	49	V	0.2	164	B, 1
Cyg OB2 3	O9:	B	51033	5.2	104	6.4	106	V	0.4	86	A, 2
(BD+40 4212)						5.2	106	R			4
						5.8	104	V			8
						5.3	106	R			13
						6.0	106	O			6
Cyg OB2 5	O7Ianfp	B	51033	3.6	80	3.5	84	R	0.4	86	E, 13
(BD+40 4220)			51034	3.3	81	4.4	85	V			8
			total	3.4	81	4.0	80	V			2
						3.2	84	O			6

Spectral-type sources: A, Hiltner (1956); B, Mathys (1989); C, Walborn (1972); D, Walborn (1973a); E, Walborn (1973b); F, Walborn (1976).

Photopolarimetry sources: 1, Guetter & Vrba (1989); 2, Hiltner (1956); 3, Klare & Neckel (1977); 4, Kobulnicky et al. (1994); 5, Lupie & Nordsieck (1987); 6, McMillan & Tapia (1977; $O \simeq R$); 7, Östreicher & Schulte-Ladbeck (1982); 8, Serkowski (1965); 9, Serkowski (1968); 10, Serkowski, Mathewson & Ford (1975); 11, Serkowski & Robertson (1969); 12, van Smith (1956; wavelength unspecified); 13, Whittet et al. (1992).

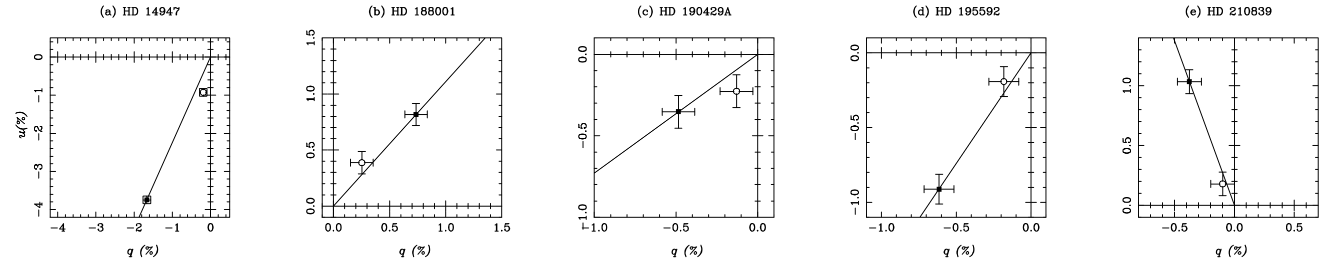

Figure 2. Optical (filled squares) and K-band (open circles) continuum polarization measurements plotted in the QU plane. The solid line in each panel is a straight line passing through the optical data point and the origin, and indicates the interstellar polarization vector assuming zero intrinsic polarization.

3.3 Notes on individual targets

3.3.1 HD 108.

The continuum polarization of this target closely matches that of the nearest field stars (Figure 4a), suggesting that the bulk of the polarimetric signal is interstellar in origin. However, the Hα profile (Figure 3a;) reveals a small but statistically significant rotation in PA through the line, as well as marginal evidence for an enhancement in polarization magnitude. A photopolarimetric time-series by Fox & Hines (1998) shows evidence for systematic variability in $p(\lambda)$ at the 0.2% level on intranight timescales, which they interpreted as the result of density inhomogeneities passing through a rotating, face-on disk. Our two measurements of this object, separated by one day, show no evidence for variability and are in reasonable agreement with published data (Table 2).

3.3.2 HD 14947.

The ISP structure of field stars is well defined (Figure 4b), and the continuum polarization of the target is consistent with this pattern. The high-S/N polarization spectrum (Figure 3b) is contaminated by residual instrumental ripple, but there is no evidence for a change in the polarization vector across Hα. Our two measurements of this target show marginal evidence for variability, and the polarization magnitude is significantly smaller than reported by Hiltner (1956). Our K-band measurement of this target lies close to a line in the QU plane joining the optical measurement to the origin (Fig. 2), providing further evidence that the polarization of this system is dominated by the interstellar component.

3.3.3 HD 15570.

The PA of the continuum polarization of this object is approximately aligned with that of the local ISP (Figure 4c), although its magnitude is slightly larger. The polarization spectrum is again contaminated by residual instrumental ripple, but there is a suggestion of enhanced polarization magnitude across the emission line (Figure 3c).

Our measurement of the polarization magnitude agrees with that reported by Guetter & Vrba (1989), but Hiltner's (1956) value is much larger (Table 2). Since Hiltner's PA measurement is not discordant, it is possible that his tabulated value is a misprint, although since he tabulates the polarization as a logarithmic magnitude it is not simply that 5.4% has been misprinted as 6.4%. His 1956 value appears to be a copy of a result originally published five years earlier (Hiltner 1951), where he gave the polarization both as a logarithmic magnitude and a percentage[1] (0.131m, 6.0%); however, if the latter figure is derived from the former, then transposing two digits could give (0.113m, 5.5%), potentially reconciling all results.

3.3.4 HD 30614 (α Cam).

There are few field stars catalogued nearby to HD 30614, but it appears that its continuum polarization is roughly consistent with those stars available (Figure 4d). After correction for the (fairly severe) instrumental ripple it appears that the polarization is sensibly constant through Hα (Figure 3d), although Hayes (1984) and Lupie & Nordsieck (1987) report continuum polarization variability at the $\sim$0.1% level.

3.3.5 HD 149404 (V918 Sco).

This double-lined spectroscopic binary ($P_{\rm orb} = 9.8$d) shows a strong depolarization at Hα with a corresponding change in PA (Figure 3e). The continuum polarization has both a larger magnitude and a different orientation to the local ISP (Figure 4e). The observed line effect may arise from intra-binary scattering, especially since the system shows phase-related polarization variability at the $\sim$1% level (Luna 1988).

3.3.6 HD 151804.

Although the continuum polarization of this object appears to be consistent with the ISP field (Figure 4f), there is marginal evidence for a change in polarization angle at Hα (Figure 3f).

[1] We have converted polarizations in the older literature, expressed in magnitudes, to percentage polarizations by using $p(\%) = 100 \times [(10^{0.4p(\Delta m)} - 1)/2]$; however, this does not precisely reproduce Hiltner's transformations, which appear to be simply linear ($p(\%) = 46p(\Delta m)$; see also van Smith 1956.)

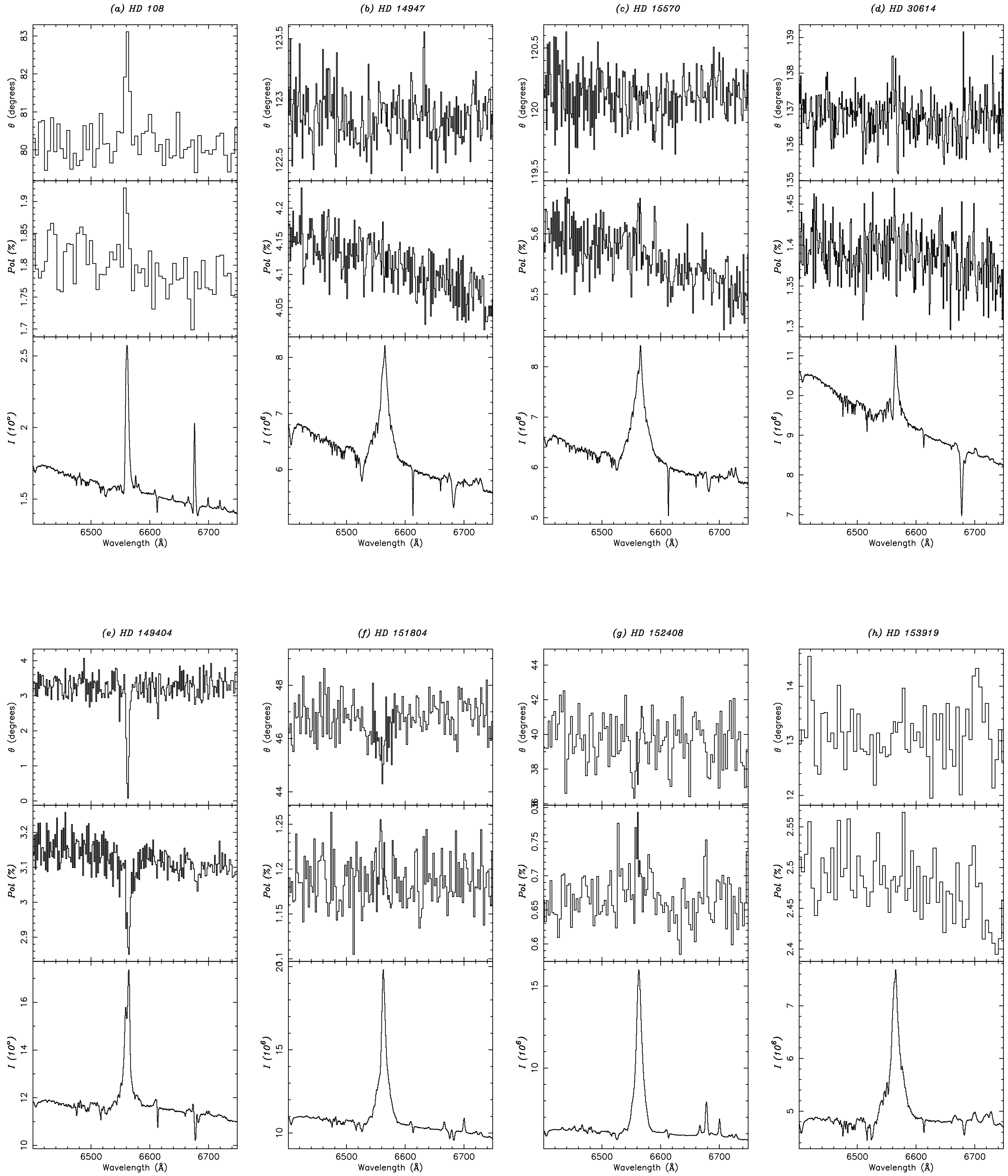

Figure 3. The spectra; polarimetric data are binned to a constant error of 0.03% in P. Summed spectra are shown for the targets which have multiple observations, and the data have been corrected with a model fit to the instrumental ripple. Most of the sharp features bluewards of line centre are telluric, and have no significant polarimetric signature; other features include He λ6680 and the 6614Å diffuse interstellar band. Note that the y ranges vary from plot to plot.

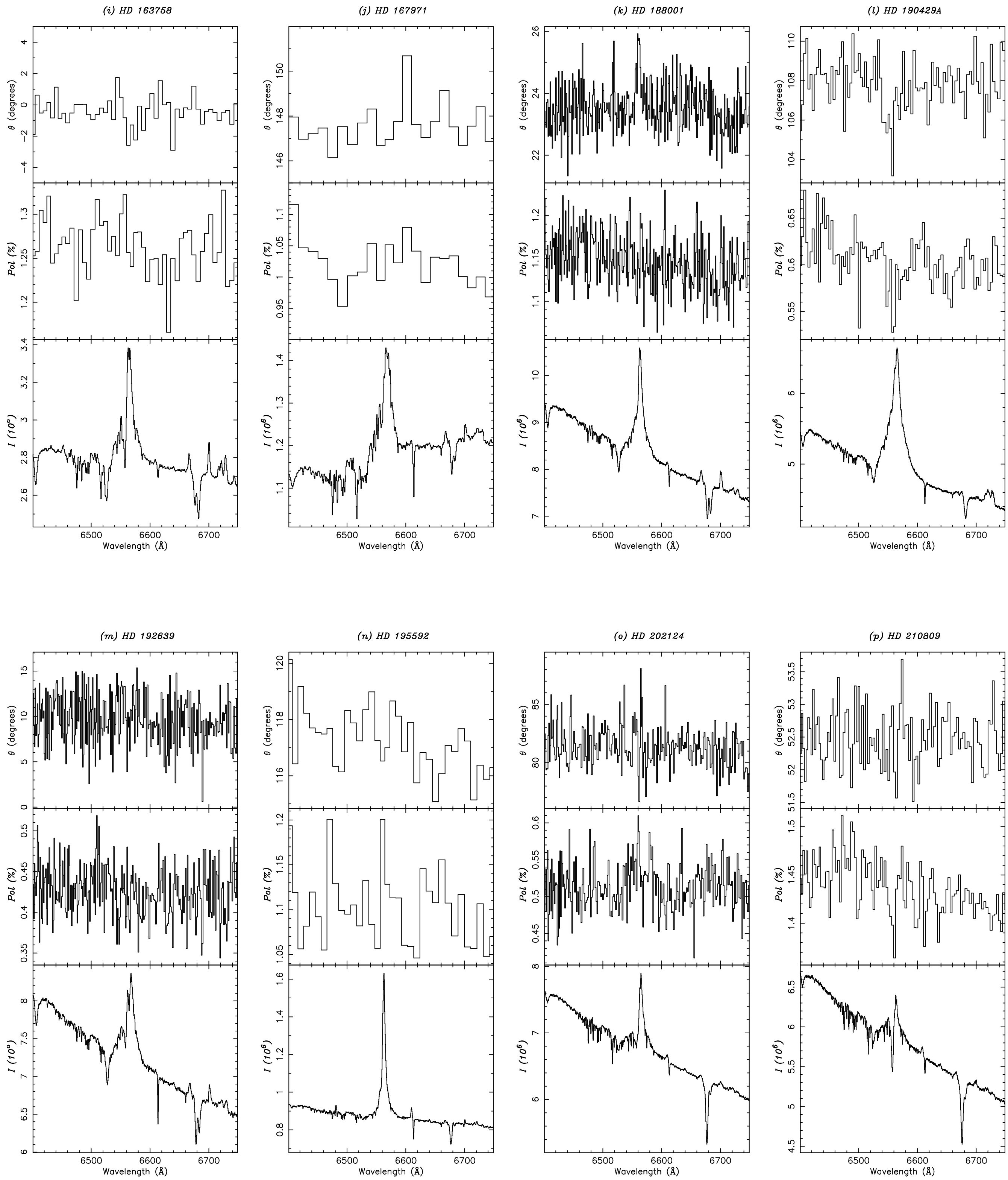

Figure 3. Continued.

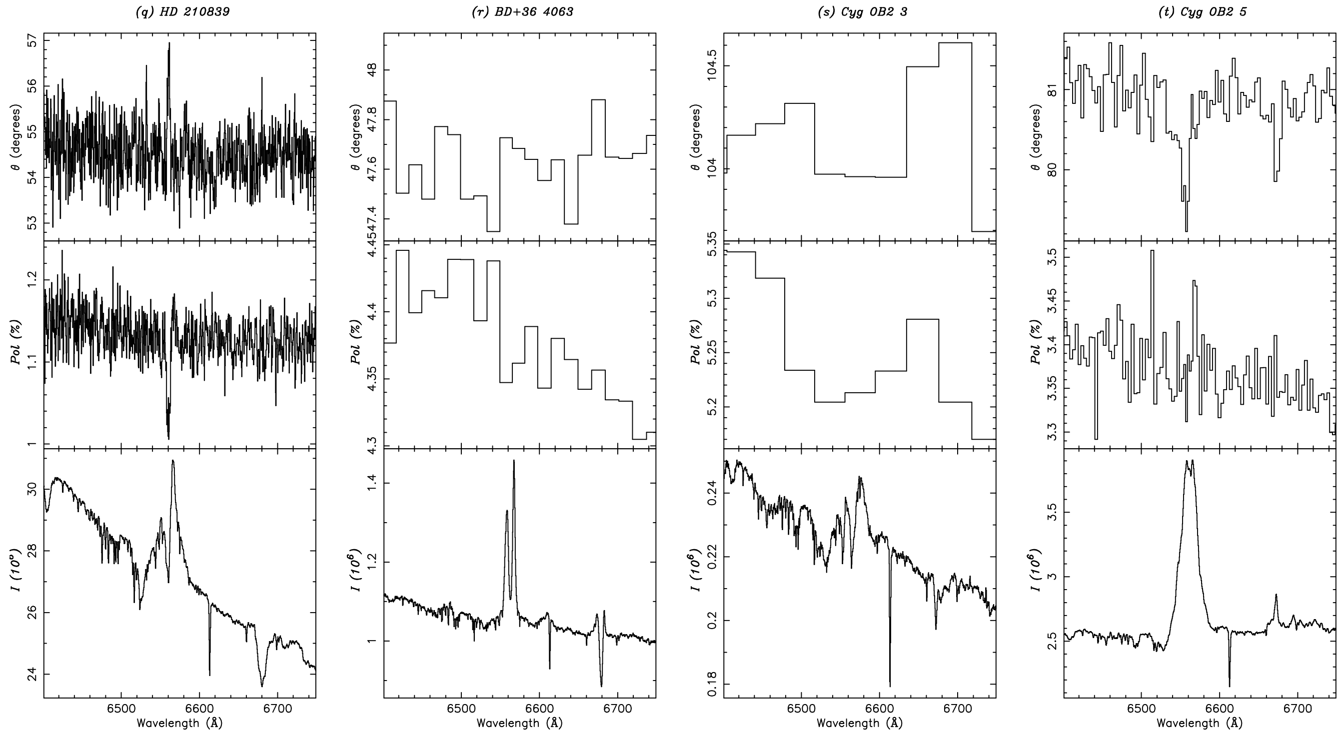

Figure 3. Continued.

3.3.7 HD 152408.

The continuum polarization agrees well with the local ISP pattern (Figure 4g), but there appears to be slight evidence of a PA rotation in combination with a magnitude enhancement across Hα (Figure 3g).

3.3.8 HD 153919 (V884 Sco).

This is the optical companion to the X-ray source 4U1700 − 37. Although the continuum polarization is quite different to the local ISP structure (Figure 4h), the polarization at Hα is the same as that of the continuum (Figure 3h). The system shows orbital polarization variability at the ∼0.3% level (e.g., Dolan & Tapia 1984).

3.3.9 HD 163758.

There is no evidence of Hα polarization structure in this object (Figure 3i) and the continuum polarization is consistent with that of the surrounding field stars (Figure 4i).

3.3.10 HD 167971 (MY Ser).

The local ISP structure is not well ordered (Figure 4j), but the continuum polarization does closely match that of the nearest field star. There is no evidence of Hα polarization structure (Figure 3j).

3.3.11 HD 188001 (9 Sge).

The continuum polarization is aligned with the ISP of two of the nearby field stars (Figure 4k). An Hα line effect is observed in the PA spectrum after subtraction of the ripple pattern (Figure 3k). Hayes (1975) reports internight photopolarimetric variability with an amplitude of ∼0.2% ($\sigma_{\rm p}$ = 0.08%). When our K-band point is plotted in the QU plane (see Fig. 2b) it lies on a line joining the optical datum to the origin, indicating the polarization is mostly interstellar in origin.

3.3.12 HD 190429A.

The local ISP pattern is chaotic (Figure 4l). The polarization spectrum is affected by the instrumental ripple (Figure 3l), but there appears to be marginal evidence for a polarization decrease at Hα after ripple correction. The 'B' companion is 1.96″ distant at PA 174° and is 0.6m fainter (ESA 1997); our observation was carried out in good (0.8″), stable seeing. Comparing the optical and IR continuum measurement (Fig. 2c) we see that the intrinsic component to the polarization must be small compared to the ISP.

3.3.13 HD 192639.

Once again the local ISP pattern is unstructured (Figure 4m). There is no evidence for Hα polarization structure (Figure 3m), but the spectrum is affected by residual instrumental ripple.

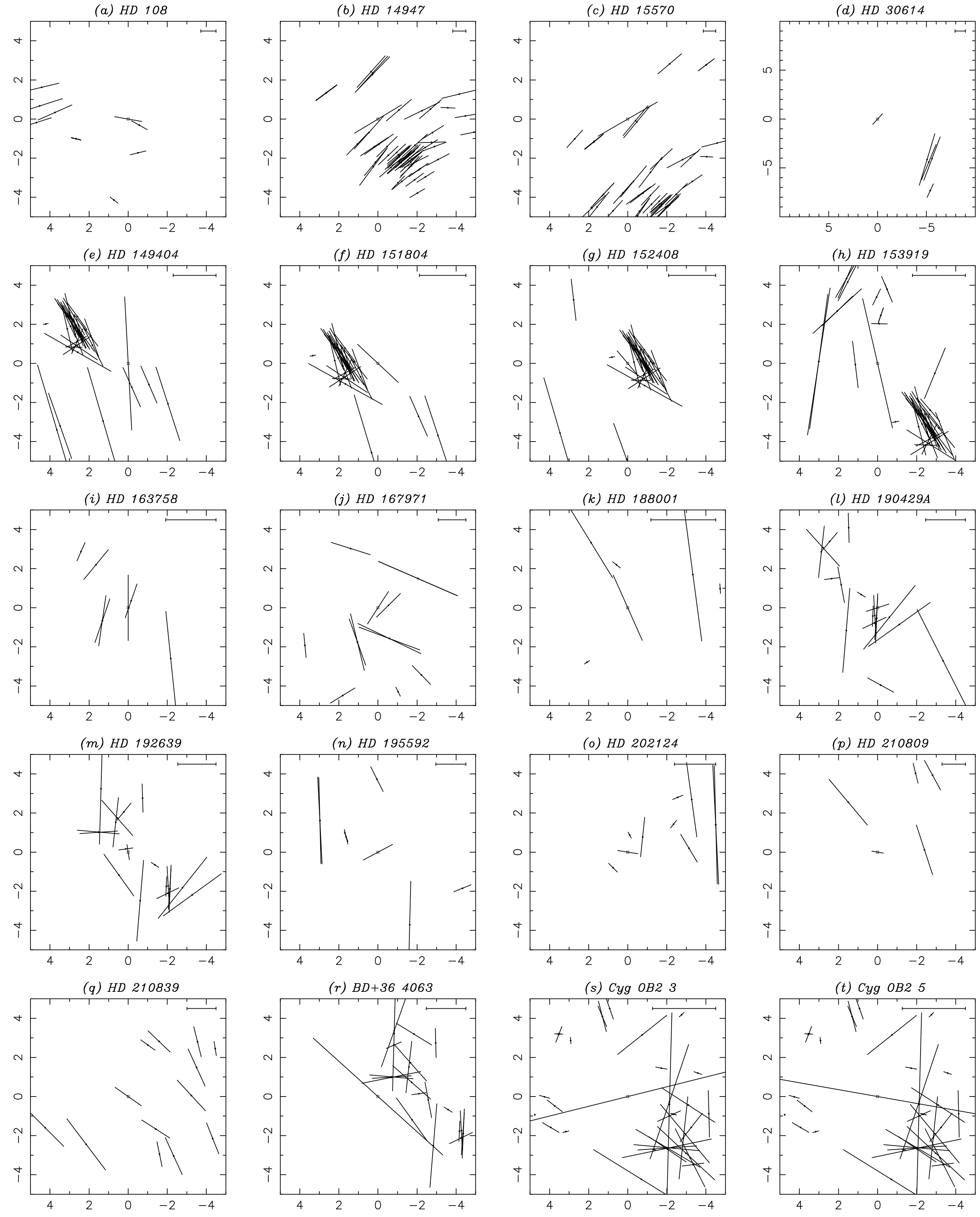

Figure 4. Interstellar polarization maps around the target stars. The axes of the maps are RA (abscissa) and declination (ordinate) and are in units of degrees from the target position. The bar at the top right of each figure represents 1% polarization, and the continuum polarization of the target is plotted at $(0, 0)$.

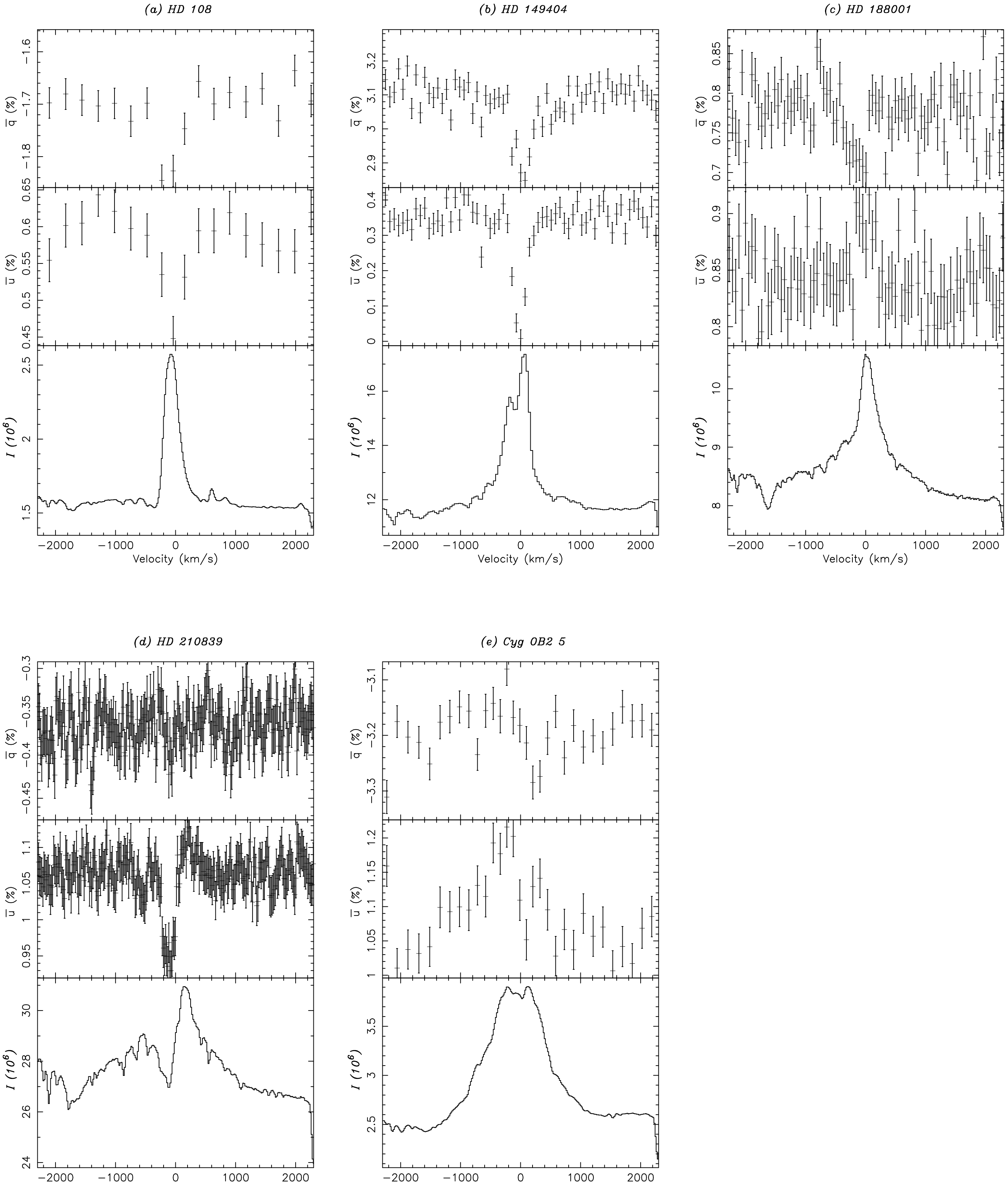

Figure 5. (a)-(e). Polarization spectra of the targets with a statistically significant measurement of a line effect. The data are binned to a constant error of 0.03% in P, and are plotted in observed velocity-space.

3.3.14 HD 195592.

The ISP map is sparsely populated (Figure 4n). The polarization spectrum shows no evidence for a polarization change through Hα (Figure 3n). Our observations of this target, taken a day apart, show no significant variability. The K-band measurement lies on a line joining the optical QU point to the origin (see Fig. 2d), which strongly suggests that the continuum polarization is dominated by ISP.

3.3.15 HD 202124.

The local ISP field is poorly ordered (Figure 4o), while the polarization spectrum shows no evidence of Hα polarization structure (Figure 3o).

3.3.16 HD 210809.

Although the raw data are dominated by instrumental ripple, there is marginal evidence in the polarization spectrum for a change in polarization magnitude at Hα, which persists in the ripple-corrected spectrum (Figure 3p). Although only a few cospatial field stars were found in the catalogue, the ISP pattern is fairly well-defined and is inconsistent with the target's continuum polarization (Figure 4p).

3.3.17 HD 210839 (λ Cep).

Hayes (1975) reports internight variations in polarization at the 0.2% level. The summed spectrum of this object suffers from instrumental ripple, but a depolarization at Hα is evident, combined with a PA rotation (Figure 3q). The continuum polarization closely matches those of the nearby field stars (Figure 4q), and optical and K-band continuum polarization (Fig. 2e) confirms that the interstellar medium is the dominant polarigenic source for this system.

3.3.18 BD+36 4063.

This is a single-lined spectroscopic binary ($P_{\rm orb} = 4.8$d), showing large orbital changes in its Hα profile (Howarth et al., in preparation). At the time of our observations the continuum polarization was relatively large (4.4%, Table 2), and significantly greater than expected from the surrounding field stars (Figure 4r), which, however, show no well-defined pattern. The polarization spectrum shows a sharp drop in polarization centred on the redwards Hα peak (Figure 3r). The difference in R-band polarization between our observation and that reported by Guetter & Vrba (1989) is large enough to suggest the possibility of (orbital?) variability.

3.3.19 Cyg OB2 3 (BD+40 4212).

This star also shows substantial Hα variability, which is probably related to binary interaction (Howarth, unpublished). The continuum polarization is the largest recorded in our sample (5.2%, Table 2). The local ISP is chaotic (Figure 4s; see also the detailed photopolarimetric study by Kobulnicky, Molnar & Jones 1994, and references therein). The polarization does not change significantly across Hα in our (relatively poor) data. Published values of V- and R-band polarization show a dispersion in excess of 5.2–6.4%, strongly suggesting (orbital?) variability.

Table 4. HPOL measurements of HD 108, HD 188001, and λ Cep . The columns refer to the date of the observation, the continuum polarization (summed over the entire wavelength range) as normalized Stokes parameters (q, u).

Date	q (%)	u (%)
	HD 108	
1991 Sep 08	-1.682 ± 0.012	0.632 ± 0.012
1991 Sep 11	-1.569 ± 0.012	0.557 ± 0.012
1996 Sep 18	-1.635 ± 0.011	0.540 ± 0.011
1996 Oct 15	-1.592 ± 0.008	0.477 ± 0.008
1996 Oct 20	-1.673 ± 0.014	0.525 ± 0.014
	HD 188001 (9 Sge)	
1989 Aug 11	0.602 ± 0.014	0.877 ± 0.014
1989 Oct 12	0.838 ± 0.009	0.859 ± 0.009
1989 Dec 06	0.621 ± 0.040	0.852 ± 0.040
1990 May 11	0.618 ± 0.006	0.905 ± 0.006
1990 Jul 01	0.699 ± 0.012	0.854 ± 0.009
1990 Aug 12	0.724 ± 0.007	0.860 ± 0.007
1991 Feb 25	0.686 ± 0.017	0.868 ± 0.017
1991 May 28	0.765 ± 0.012	0.848 ± 0.012
	HD 210839 (λ Cep)	
1991 Oct 18	-0.438 ± 0.004	1.047 ± 0.004
1991 Oct 22	-0.381 ± 0.005	1.025 ± 0.005
1991 Oct 23	-0.471 ± 0.004	0.998 ± 0.004
1994 Aug 20	-0.425 ± 0.005	0.995 ± 0.005
1994 Oct 21	-0.438 ± 0.004	1.047 ± 0.004
1994 Nov 24	-0.439 ± 0.009	1.056 ± 0.009
1995 Sep 02	-0.408 ± 0.008	1.083 ± 0.008
1995 Sep 27	-0.521 ± 0.005	1.086 ± 0.008
1995 Oct 12	-0.460 ± 0.007	1.101 ± 0.007

3.3.20 Cyg OB2 5 (BD+40 4220, V729 Cyg).

The continuum polarization of this object is aligned to within 20° of Cyg OB2 3, but its magnitude is lower. A small PA rotation is observed across Hα (Figure 3t), showing that an intrinsic polarization is present. This star is a double-lined eclipsing spectroscopic binary (e.g., Rauw, Vreux & Bohannan 1999); our two observations taken a day apart show a decrease in polarization magnitude which is formally significant; the spread in published photopolarimetric results (Table 2) is also large enough to suggest significant intrinsic (orbital?) variability.

4 DISCUSSION

Five of our 20 systems (25%) show a statistically significant change in polarization through Hα. Two of these systems are known binaries (HD 149404 and Cyg OB2 5) while the remaining objects are thought to be single. Although some of the spectropolarimetry suggests a classical line dilution effect (cf. HD 108 and HD 149404), others are obviously more complex (e.g. HD 210839). In the following sections we exam the Hα polarization morphology of each of these five objects in detail.

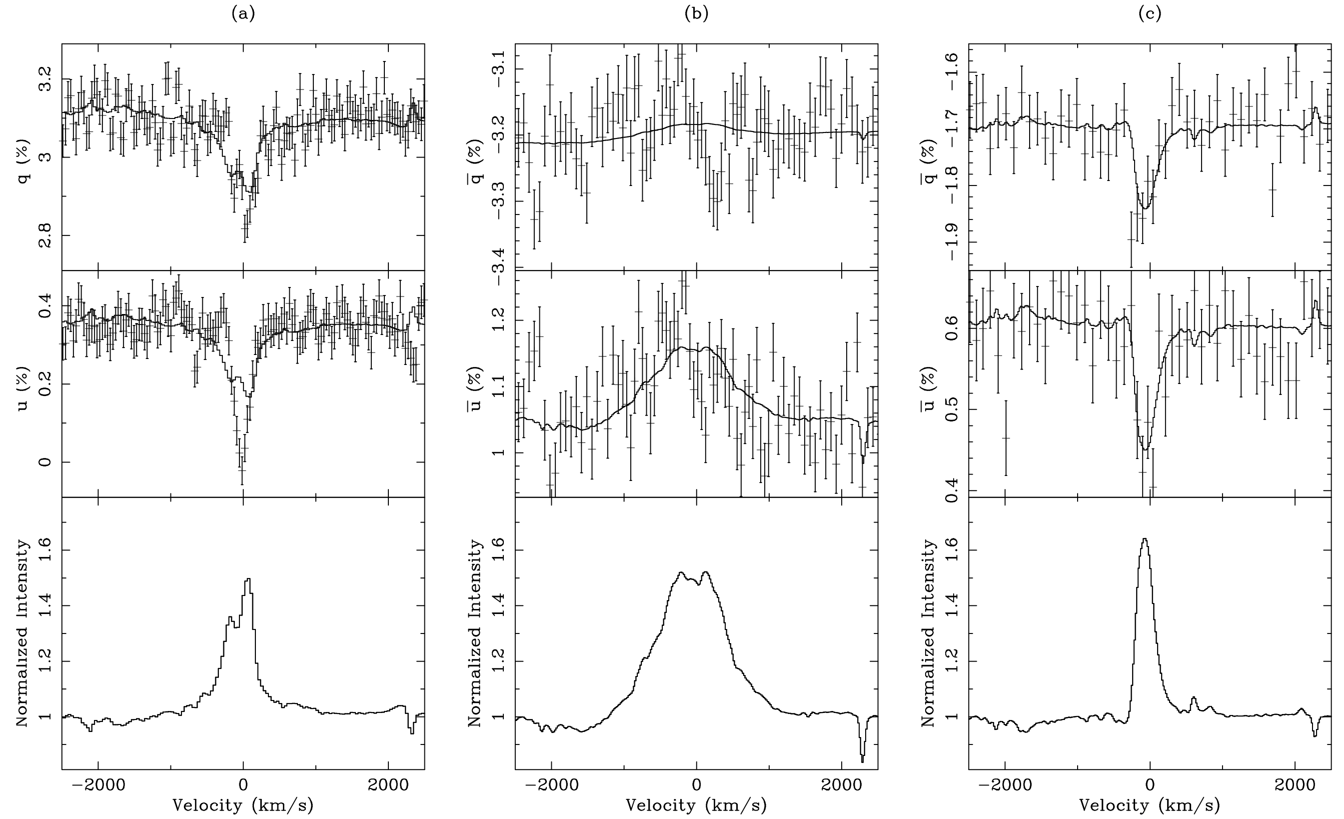

Figure 6. The normalized Hα spectrum (solid line, bottom panel), plus the normalized Stokes Q and U spectra (error bars, top and middle panels repsectively) of (a) HD 149404, (b) Cyg OB2 5, and (c) HD 108. Also plotted (solid line, top and middle panels) are the fits detailed in Sections 4.1, 4.2, and 4.3.

4.1 HD 149404

HD 149404 is a 9.8 d-period massive binary that shows evidence (particularly in Hα line-profile morphology) for colliding-wind interaction (Thaller et al. 2001). Polarimetric variations (Luna 1988) and light-curve analyses of the ellipsiodal variations (e.g. Penny et al. 1996) indicate a low inclination, and by comparing the minimum masses from radial-velocity measurements and the canonical masses of the two components from their spectral types, Rauw et al. (2001) estimated an orbital inclination of 21°. The secondary (the brighter, but less massive component) is close to filling its Roche lobe, but it appears that the stars are rotating super-synchronously (Penny et al. 1996), which would rule out a semi-detached configuration. The geometry and dynamics of the colliding wind region is uncertain, with Thaller et al. (2001) proposing that the bulk of the Hα arises from a volume between the stars, while Rauw et al. (2001) suggest that the emission arises in two localized regions downstream of strong shock front and exterior to the binary orbit.

HD 149404 shows the classical line dilution effect (Fig. 5b), with the continuum polarization resulting from scattering of the radiation of one component in the wind or photosphere of its companion, leading to strong polarimetric variation in the second harmonic of the orbital period (Luna 1988). The Hα profile shows a double-peaked signature, and is relatively strong (~ 1.5 relative to the continuum).

A simple dilution model predicts that the intrinsic polarization spectrum through Hα is

$$s(\lambda) = s_c / I(\lambda) \tag{3}$$

where $s(\lambda)$ is the normalized Stokes intensity (q or u), s_c is the continuum value of the normalized Stokes intensity, and $I(\lambda)$ is the normalized intensity spectrum. We fitted this equation, plus a modified Serkowski law to our spectropolarimetry, fixing $\lambda_{\max}$ at the canonical value of 5500Å (we do not have sufficient wavelength coverage in our high resolution data to constrain the shape of the ISP law properly). The resulting fit (reduced $\overline{\chi^2} = 1.2$, Figure 6a) yields an interstellar polarization of $2.60 \pm 0.4\%$ at a PA of $177.5 \pm 0.4°$, with a continuum polarization of $0.83 \pm 0.03\%$ at $22 \pm 1°$. Although the fit is reasonable in the line wings, descrepancies near the line centre are indicative of secondary polarigenic effects. Such departures from pure dilution may be due to the presence of significant photospheric Hα absorption, or line absorption of continuum photons. Detailed radiative transfer modelling of this system is beyond the scope of the present paper.

4.2 Cyg OB2 5 (V729 Cyg)

The polarigenic mechanism in this spectroscopic binary is almost certainly classical dilution, with the apparent *increase* in polarization magnitude through the line arising from a chance alignment of the intrinsic and foreground polarizations. Fitting eqtn. 3 to our $H\alpha$ polarization spectrum (fixing $\lambda_{\max} = 5500$Å) we find $\overline{\chi^2} = 0.66$ and an interstellar vector of $3.56 \pm 0.05\%$ at $78.2 \pm 0.3°$ (see Figure 6b).

This large magnitude for the ISP component is consistent with the object's high reddening (an $E(B-V)$ of two magnitudes). The intrinsic component determined from the fit ($0.32\pm0.03\%$ at $139\pm3°$) is certainly consistent with our binary scattering interpretation, which can be tested by using time-series photopolarimetry.

4.3 HD 108

The line effect observed in HD 108 (Fig. 5a) could certainly be associated with a low level (0.2 to 0.3%; e.g. Fox & Hines 1998) of continuum polarization. The width of the line effect observed is comparable with that of the intensity profile, as expected if the Hα emission is unpolarized and the morphology results from pure dilution. Interestingly, there is no evidence for a depolarization through the strong He I λ6678 emission line, perhaps because this line is produced over a smaller volume than Hα.

We fitted eqtn. 3 plus a modified Serkowski law (eqtn. 2) to the HD 108 polarization spectrum. Since the wavelength range is small, we once again fixed $\lambda_{\rm max}$ to the canonical value of 5500Å. The ISP derived from this fit is $p_{\rm max} = 2.14\pm0.06\%$ at a PA of $87\pm1°$, with a intrinsic continuum polarization of $0.54\pm0.06\%$ at $23\pm3°$. The fit is good, with $\overline{\chi^2} = 0.55$ (Figure 6c), and matches the line width particularly well. In part this is due to the relative strength of the Hα emission line in this system, which masks secondary effects such as photospheric absorption (cf. HD 149404).

We used archive data from the Pine Bluff Observatory spectropolarimeter (HPOL) in an attempt to constrain better the interstellar polarization. These data are low resolution and extend from 3200–7700Å. A λ-independent (electron scattering) intrinsic polarization plus modified Serkowski law was fitted to all the data simultaneously, which yielded $p_{\rm max} = 2.58\pm0.03\%$ at $78.7\pm0.3°$ with $\lambda_{\rm max} = 5380\pm15$Å, and a continuum polarization of $0.66\pm0.03\%$ at $162\pm1°$. This fit ($\overline{\chi^2}$=1.18) is good, although the orthogonal intrinsic and ISP position angles argue against this being physically meaningful solution. [The orthogonality is driven by the fact that the observed PA is (to first order) wavelength independent; hence any substantial intrinsic polarization must be aligned with, or at 90° to, the ISP angle.] A further fit, with the intrinsic polarization held at the value indicated by the dilution model, yielded $p_{\rm max} = 2.22\pm0.003$ at $88\pm0.1°$ with $\lambda_{\rm max} = 5370\pm14$Å. With $\overline{\chi^2} = 1.25$, the fit is inevitably worse and cannot reproduce the observed flat PA spectrum.

We believe that classical dilution is the best explanation of the Hα data, but the presence of significant polarization variability means that it is not possible to create a self-consistent model for the intrinsic polarization component with the current dataset. Cotemporaneous high-resolution and low-resolution spectropolarimetry are required, and data in the K-band (where the contribution of the interstellar polarization is much reduced in comparison to the electron-scattering intrinsic polarization) would provide additional leverage on the fits detailed above.

4.4 HD 188001 (9 Sge)

The Hα polarization morphology is intriguing, since the change is broad (comparable with the FWZI of the Stokes I emission profile) and there appears to be a polarization rotation across the blue line wing. We found that a simple dilution model, as used for HD 108 (cf. Section 4.3) cannot reproduce the observed polarization structure. However, HD 188001 does not have a particularly rapid projected rotation speed ($v_e \sin i = 93\,{\rm km\,s^{-1}}$; Howarth et al. 1997), so we cannot invoke the ζ Puppis line absorption effect (see Section 4.5 for details). The relative intensity of the Hα line in HD 188001 is about a factor of two smaller than HD 108 and HD 149404, and in this case the detailed properties of the line formation (the depth of the Hα absorption, line absorption of continuum photons etc) play a critical role in producing polarization structure through the line (Harries 2000).

There are eight low-resolution observations of HD 188001 in the HPOL archive (see Table 4), and we fitted these with a constant, wavelength-independent intrinsic component plus a modified Serkowski law (eqtn. 2). The Serkowski law has a maximum polarization of $1.35\pm0.05\%$ at $25\pm1°$, at a wavelength of 5770 ± 40Å, and the intrinsic component is $0.13\pm0.05\%$ at a PA of $113\pm11°$. The fit is relatively poor ($\overline{\chi^2} = 2.18$), and a fit neglecting the intrinsic component shows that a single modified Serkowski law fits the data equally well. Our K-band observation is also most easily interpreted in terms of foreground polarization (see Fig. 2b). We therefore rule out a significant temporally-constant intrinsic polarization, and suggest that the low-level ($\sim 0.1\%$) level of polarization variability observed in the HPOL data and the photopolarimetry of Hayes (1975) is produced by stochastic changes in the density structure (clumps) of the stellar wind.

4.5 HD 210839 (λ Cep)

The observation of λ Cep (HD 210839) is of high S/N and striking polarimetric changes are observed through the line profile (Fig. 5d) while the photopolarimetric data, such as our K-band point (Fig. 2e) and V-band timeseries (Clarke et al. 2002), are consistent with a zero intrinsic continuum polarization. These data do not, however, rule out the possibility of a significant *constant* intrinsic polarization, although fits of a modified Serkowski law (eqtn. 2) to broad-band photopolarimetry by McDavid (2000) indicate that such a component should be small. We investigated this using HPOL data. Nine observations were employed, three nights in each of 1991, 1994 and 1995. A summary of the data is given in Table 4, along with the polarization measured across the entire wavelength range. Inspection of the mean polarizations confirm that the variability is small on a night-to-night basis and is very stable over a three year period.

We fitted the HPOL data with a single modified Serkowski law (eqtn. 2) plus a λ-independent offset (p_0, θ_0). This resulted in a fit with $\overline{\chi^2} = 1.64$, $p_{\rm max} = 1.08\pm0.02\%$, $\theta_{\rm isp} = 48.7\pm0.5°$, $\lambda_{\rm max} = 5181\pm12$Å. The offset is $0.32\pm0.02\%$ at $87\pm2°$. Extrapolating the modified Serkowsi law to the K-band and subtracting it from our UKIRT measurement we get an intrinsic polarization of $0.07\pm0.37\%$ at a position angle of $91\pm12°$, which suggests that the intrinsic polarization derived from the optical HPOL data is not consistent with the near-IR measurement. Forcing the fit to pass through the K-band point we find a negligible intrinsic polarization (0.03%) and an interstellar law ($p_{\rm max} = 1.18\%$,

Table 5. Physical parameters of λ Cep adopted for the numerical model. The values were taken from Puls et al. (1996), excepting $v \sin i$ (taken from Howarth et al. 1997).

Parameter	Value
v_0 ($\mathrm{km\,s^{-1}}$)	10
v_∞ ($\mathrm{km\,s^{-1}}$)	2250
β	0.9
$v \sin i$ ($\mathrm{km\,s^{-1}}$)	219
Mass-loss rate ($\mathrm{M_\odot yr^{-1}}$)	5.3×10^{-6}
R ($\mathrm{R_\odot}$)	19
$T_{\rm eff}$ (K)	38 000

$\theta_{\rm isp} = 55.7°$, $\lambda_{\rm max} = 5025$Å) that is almost indistinguishable from that found by McDavid (2000). We therefore conclude that there is no detectable gray (electron scattering) continuum polarization in λ Cep.

This implies that the polarization change observed through Hα is not a classical line effect (i.e. dilution of a polarized continuum by unpolarized Hα emission). The change in polarization is narrow ($\sim 230\,\mathrm{km\,s^{-1}}$), and is centred close to zero velocity ($\sim -30\,\mathrm{km\,s^{-1}}$) after correction for the systemic velocity of $-74\,\mathrm{km\,s^{-1}}$(Underhill 1995). We propose that this morphology may result from a line-transfer effect due to rapid rotation (cf. ζ Puppis, Harries 2000) in which continuum photons are absorbed by the line. In order to test this hypothesis we created a synthetic Hα line profile using the TORUS radiative-transfer code (Harries 2000).

We used the physical parameters for λ Cep listed in Table 5, and the Hα source function was computed using the approximation to the $n = 2$ and $n = 3$ departure coefficients given by Puls et al. (1996). The rotational velocity field was computed according to conservation of angular momentum (Harries 2000), while the radial flow was described by the usual β-law. The model is core–halo, and to estimate the absorption component of the line we adopted the procedure described in Paper I, in which the core profile is chosen so that the emission line intensity closely matches the observation.

Comparison between the model and the observation was made by subtracting the continuum polarization from the observation, and rotating the model PA until all the information is in the U Stokes parameter (as per the observation). Figure 7 shows a comparison between the observation (Figure 7a) and the model computed using the parameters listed in Table 5 (Figure 7b). Although the intensity and red wing of the model line profile are in approximate agreement with the observation the presence of the rotation in the model changes the details of the line shape (we stress that this is not a fit to the observation). The polarized line profile shows qualitative agreement, in that there is a decrease in polarization close to zero velocity, the width of the polarization dip is comparable to the rotational velocity, and there is a polarization enhancement on either side of the dip. Quantitively the model is less convincing, since the depth of the polarization dip is too small (by approximately a factor two), although its width ($\sim 200\,\mathrm{km\,s^{-1}}$) and central velocity ($-60\,\mathrm{km\,s^{-1}}$) are in reasonable agreement with the observations.

In order to get a deeper polarization dip it is necessary to increase the line opacity at low velocity, where the azimuthal component of the velocity field dominates the radial. We attempted this by increasing the β index of the velocity law (from 0.9 to 1.15) and reducing the mass-loss rate to $5 \times 10^{-6}\mathrm{M_\odot\,yr^{-1}}$ (to retain a reasonable line emissivity). This model (Figure 7c) does reproduce the observed polarization dip better in terms of depth, width ($\sim 210\,\mathrm{km\,s^{-1}}$), and central velocity ($\sim -30\,\mathrm{km\,s^{-1}}$). The sensitivity of the polarized line profile morphology to the adopted velocity field suggests that it may be possible to use it as a diagnostic of the wind base kinematics, although this would require a unified hydrostatic–wind boundary model rather than the core–halo construction used here.

In this model for the polarized line formation the PA of the observed polarization is the orientation of the rotation axis projected onto the plane of the sky. We measured this PA by subtracting the continuum polarization and finding the intensity-weighted mean polarization vector over a 2Å bin centred on the polarization minimum, and obtained a value of $126 \pm 2°$.

5 CONCLUSIONS

We have presented new moderate-resolution linear spectropolarimetry of the Hα emission lines of 20 O supergiant stars, of which 25 per cent show a measurable change through the line. For the binary systems we attribute the continuum polarization to the scattering of one components radiation in the wind and photosphere of its companion, and we conclude that the line effect in these systems arises from classical dilution.

By comparing our measured continuum polarization vectors with literature polarization measurements and cospatial field stars, and by using new K-band polarimetric measurements, we find that typically the intrinsic polarization in the single stars is small ($< 0.1\%$). We suggest that the line polarizations observed λ Cep arises from radiation transfer in a rotational velocity field (cf. ζ Puppis; Paper I; Harries 2000). It may be possible to use this effect both as an indicator of inclination and of the relative magnitudes of the azimuthal and radial velocity fields near the base of the stellar wind, although more complex non-core–halo models will be required to fully exploit its potential. Low resolution PBO observations, combined with our K-band data, provide strong evidence that there is no constant intrinsic polarization in λ Cep, and that the wind is therefore spherical despite the star's rapid rotation.

In order to quantify the asymmetry allowed by a (conservative) upper limit to the continuum polarization of 0.1%, we performed calculations using TORUS, assuming a plausible latitudinal dependency of the electron density N_e,

$$N_e(r, \mu) = k(1 - x\mu^2)N_e(r) \qquad (4)$$

where $\mu = \cos\theta$, θ is the polar angle, x is a constant, and k is a normalization constant chosen to conserve the spherical mass-loss rate. Using the previously adopted parameters for λ Cep (Table 5), we find that $x = 0.2$ gives a continuum polarization of 0.1%, which corresponds to an upper limit to the equator:pole density ratio of 1.25. This lends support to the idea that non-radial line radiation forces impede the formation of strong equatorial density enhancements (Owocki et al. 1996; Gayley & Owocki 2000).

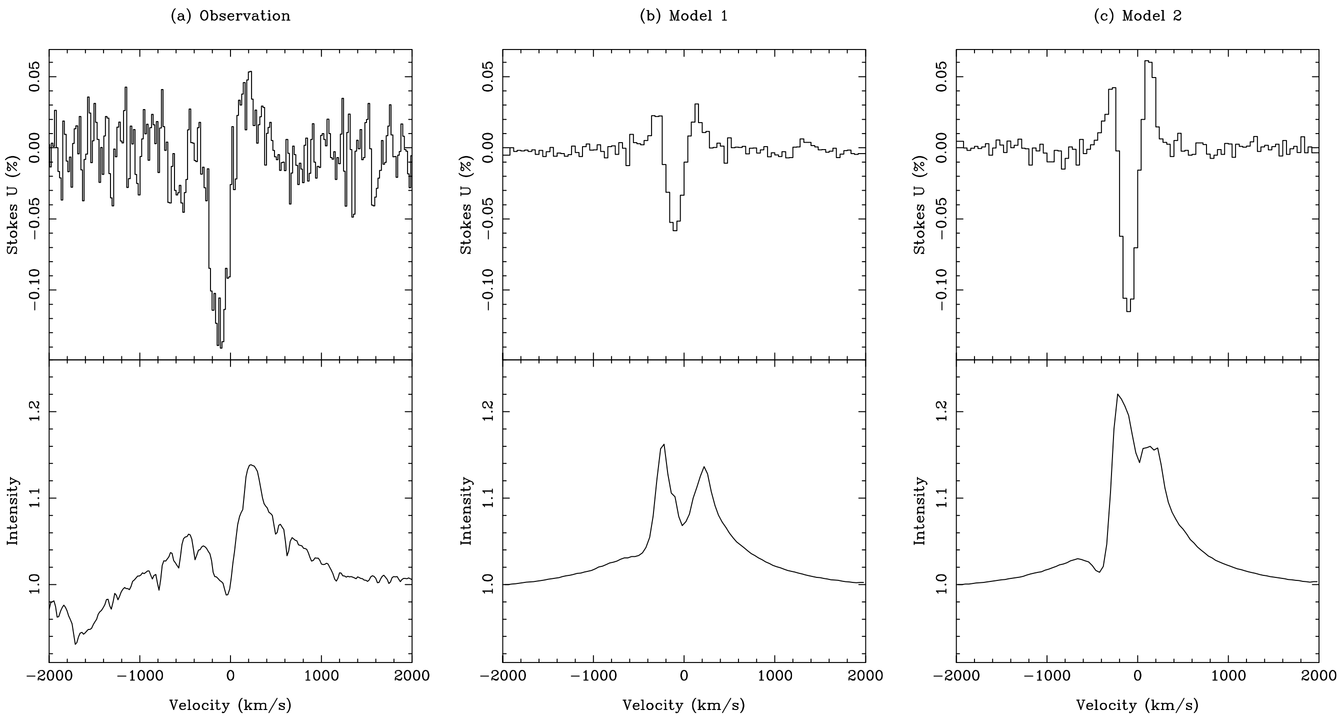

Figure 7. The intensity (lower panels) and polarization (Stokes U; upper panels) of (a) the observed Hα emission line of λ Cep (corrected for the systemic velocity of $-74\,\mathrm{km\,s^{-1}}$; Underhill 1995), (b) the $\beta = 0.9$ model, and (c) the $\beta = 1.15$ model.

Published polarimetric datasets are sensitive to intrinsic variations of greater than about 0.1%, which is unfortunately close to that predicted by radiative transfer models: Stochastic models of ζ Puppis, which are based around density enhancements propagating through the wind predict polarizations of close to 0.1–0.2% (Harries 2000) for parameters that reproduce the observed level of spectral variability (Eversberg, Lépine & Moffat 1998). A similar level of polarization variability, well correlated with line equivalent width, is expected for the co-rotating structures that are invoked to explain some UV resonance line variability. Such a correlation was tentatively claimed for 68 Cyg (McDavid 2000) but is apparently not statistically significant (Clarke et al. 2002).

Extremely careful time-series observations will be necessary to place strong constraints on structured wind models, and this requires a meticulous investigation into the night-to-night polarimetric stability of the instrument (Clarke et al. 2002). Nonetheless, observations of novae have demonstrated that data of a sufficient quality to challenge the models may be obtained with the current generation of polarimeters (e.g. Naylor et al. 1996; Moffat et al. 2001).

ACKNOWLEDGEMENTS

Paul Harrison is thanked for his assistance on the AAT observing run. We are grateful to Chris Davis and Andy Adamson for their help during our UKIRT run, and for the observations they did in service mode. This work is based on data obtained at the Anglo-Australian Telescope, NSW, the William Herschel Telescope, La Palma, and the United Kingdom Infrared Telescope, Mauna Kea. We would like to thank Ken Nordsieck and Karen Bjorkman for the use of their HPOL data and the dedicated crew of PBO observers and data reducers (in particular Brian Babler) who obtained and processed the HPOL data used in this paper.

REFERENCES

Bjorkman, J.E., Cassinelli, J.P. 1992, ApJ, 409, 429
Brown, J.C., McLean, I.S. 1977, A&A, 57, 141
Castor, J.I., Abbott, D.C., Klein, R.I. 1975, ApJ, 195, 157
Clarke, D., McDavid, D., Smith, R.A., Henrichs, H.F. 2002, A&A, 383, 580
Conti, P.S., Ebbets, D.E. 1977, ApJ, 213, 438
Conti, P.S., Howarth, I.D. 1999, MNRAS, 302, 145
Dolan, J.F., Tapia, S. 1984, A&A, 139, 249
Donati, J.-F., Catala, C., Wade, G.A., Gallou, G., Delaigue, G., Rabou, P. 1999, A&AS, 134, 149
ESA, 1997, The Hiparcos and Tycho catalogues (ESA-SP1200)
Eversberg, T., Lépine, S., Moffat, A.F.J., 1998, ApJ, 494, 799
Fox, G.K, Hines, D.C. 1998, MNRAS, 295, 423
Friend, D.B., Abbott, D.C., 1986, ApJ, 311, 701
Gayley, K.G., Owocki, S.P., 2000, ApJ, 537, 461
Garmany, C.D., Conti, P.S., Chiosi, C. 1982, ApJ, 263, 777
Guetter, H.H., Vrba, F.J. 1989, AJ, 98, 611
Harries, T.J. 1996, Starlink User Note, No. 204
Harries, T.J. 2000, MNRAS, 315, 722
Harries, T.J., Howarth, I.D. 1996a, A&AS, 119, 61
Harries, T.J., Howarth, I.D. 1996b, A&A, 310, 533 (Paper I)
Harries, T.J., Hillier, D.J., Howarth, I.D. 1998, MNRAS, 296, 1072
Hayes, D.P. 1975, ApJ, 197, L55
Hayes, D.P. 1978, ApJ, 219, 952

Hayes, D.P. 1984, AJ, 89, 1219
Hiltner, W.A. 1951, ApJ, 114, 241
Hiltner, W.A. 1956, ApJS, 2, 389
Horne, K. 1986, PASP, 98, 609
Howarth, I.D., Prinja, R.K. 1989, ApJS, 69, 527
Howarth, I.D., Prinja, R.K., Massa, D. 1995, ApJ, 452, L65
Howarth, I.D., Reid, A.H.N. 1993, A&A, 279, 148
Howarth, I.D., Siebert, K.W., Hussain, G., Prinja, R.K. 1997, MNRAS, 284, 265
Klare, G., Neckel, T. 1977, A&AS, 27, 215
Kolubnicky, H.A., Molnar, L.A., Jones, T.J. 1994, AJ, 107, 1433
Luna, H.G. 1988, A&AS, 74, 427
Lupie, O., Nordsieck, K. 1987, AJ, 93, 214
Mason, B.D., Gies, D.R., Hartkopf, W.I., Bagnuolo, W.G., Brummelaar, T.T., McAlister, H.A. 1998, AJ, 115, 821
Mathewson, D.S., Ford, V.I., Klare, G., Neckel, T., Krautter, J., 1978, Bulletin CDS, 14, 115
Mathys, G. 1989, A&AS, 81, 237
McDavid, D., 2000, AJ, 119, 352
McLean, I.S. 1980, ApJ, 236, 149
McLean, I.S., Coyne, G.V., Frecker, J.E., Serkowski, K. 1979, ApJ, 228, 802
McMillan, R.S., Tapia, S. 1977, ApJ, 212, 714
Moffat, A.F.J., Manset, N., Villar-Sbaffi, A., Vincent, L., Shara, M.M., 2001, PASP, 113, 1541
Naylor, T., Koch-Miramond, L., Ringwald, F.A., Evans, A., 1996, MNRAS, 282, 873
Östreicher, R., Schulte-Ladbeck, R. 1982, A&A, 114, 328
Oudmaijer, R.D., Drew, J.E. 1999, MNRAS, 305, 166
Owocki, S.P., Cranmer, S.R., Gayley, K.G., 1996, ApJ, 472, L115
Pauldrach, A.W.A., Puls, J., Kudritzji, R.P. 1986, A&A, 164, 86
Pauldrach, A.W.A., Kudritzji, R.P., Puls, J., Butler, K., Hunsinger, J. 1994, A&A, 283, 525
Penny, L.R., Gies, D.R., Bagnuolo, W.G., 1996, in Proc. 33rd Liège International Astrophysical Colloquium, Wolf-Rayet Stars in the Framework of Stellar Evolution, ed. J.-M. Vreux et al., 289
Puls, J., Kudritzki, R.-P., Herrero, A., Pauldrach, A.W.A., Haser, S.M., Lennon, D.J., Gabler, R., Voels, S.M., Vilchez, J.M., Wachter, S., Feldmeier, A. 1996, A&A, 305, 171
Rauw, G., Vreux, J.-M., Bohannan, B. 1999, ApJ, 517, 416
Rauw, G., Naz'e, Y., Carrier, F., Burki, G., Gosset, E., Vreux, J.-M., 2001, A&A, 368, 212
Schulte-Ladbeck, R.E., Nordsieck, K.H., Taylor, M., Bjorkman, K.S., Magalhães, A.M., Wolff, M.J. 1992, ApJ, 387, 347
Schulte-Ladbeck, R.E., Clayton, G.C., Hillier, D.J., Harries, T.J., Howarth, I.D. 1994, ApJ, 429, 846
Serkowski, K. 1965, ApJ, 141, 1340
Serkowski, K. 1968, ApJ, 154, 115
Serkowski, K., Roberston, J.W. 1969, ApJ, 158, 441
Serkowski, K., Mathewson, D.S., Ford, V.L. 1975, ApJ, 196, 261
Shortridge, K., Meyerdierks, S., Currie, M., Clayton, M., Lockley, J., Charles, A., Davenhall, C., Taylor, M. 1998, PPARC Starlink User Note, No. 86.16
Thaller, M.L., Gies, D.R., Fullerton, A.W., Kaper, L., Wiemker, R., 2001, ApJ, 554, 1070
Tinbergen, J. 1994, Spectrum (Newsletter of the Royal Observatories), 1, 26
Tinbergen, J., Rutten, R., 1992, A Guide to WHT Spectropolarimetry, ING User Manual, No. XXI
Underhill, A.B., 1995, ApJS, 100, 461
van Smith, E.P., 1956, ApJ, 124, 43
Walborn, N.R. 1972, AJ, 77, 312
Walborn, N.R. 1973a, AJ, 78, 1067
Walborn, N.R. 1973b, ApJ, 180, L35
Walborn, N.R. 1976, ApJ, 205, 419
Whittet, D.C.B., Martin, P.G., Hough, J.H., Rouse, M.F., Bailey, J.A., Axon, D.J. 1992, ApJ, 386, 562